Reconstruction of Ligaments and Droplets Via Multiview Digital Inline Holography

Weixiao Shang
School of Mechanical Engineering,
Purdue University,
West Lafayette, IN 47907

Mateo Gomez
School of Mechanical Engineering,
Purdue University,
West Lafayette, IN 47907

Terrence R. Meyer
School of Mechanical Engineering,
Purdue University,
West Lafayette, IN 47907

Sukesh Roy
Spectral Energies, LLC
Beavercreek, OH 45430

Jun Chen[1]
School of Mechanical Engineering,
Purdue University,
West Lafayette, IN 47907
e-mail: junchen@purdue.edu

Digital inline holography (DIH) is a three-dimensional (3D) measurement technique widely used in the characterizations of particles, droplets, and bubbly flows. When collimated coherent light passes an object field, the disturbed and undisturbed components will superimpose at the imaging plane and form an interference pattern (hologram) due to their phase variation. By analyzing the phase information encoded in the hologram, the shapes and locations of objects can be reconstructed. However, the reconstruction produces higher levels of uncertainty along the line of sight, which is the out-of-plane direction normal to the imaging plane. Additionally, the reconstructions algorithm cannot resolve structures blocked by other features along the recording path. To overcome these limitations, prior works have implemented DIH from two to three views on simple geometries. In this work, multiview digital inline holography is presented with (≥ 3) views to enable the reconstruction of 3D structures with complex surface topologies, including ligaments and droplets during the primary liquid breakup. The approach is similar to DIH but with a different postprocessing method that combines the information on 3D edge outlines extracted from different DIH viewing angles. Two reconstruction approaches, an outline-based method, and another cross section-based method, are developed and applied on holograms of a 3D-printed test model imitating droplet breakup. With only three views, both methods provide limited reconstruction results with various artifacts. The outline-based method uses more spatial information but, due to practical limitations, results in lower-fidelity reconstructions than the cross section-based method. In general, DIH reconstructions struggle with concave structures even with more than six views due to shadowing of obstructed structures. However, when the number of views increases to six, the cross section-based reconstruction method yields morphological details close to the test model. [DOI: 10.1115/1.4053575]

1 Introduction

The droplet breakup process and the resulting droplet size and distribution affect key performance parameters in many engineering applications, e.g., volumetric heat release rates, ignition, and burning characteristics, exhaust emissions, and soot volume fraction [1,2]. Large ligaments are procedurally broken down into smaller droplets with a characteristic size and velocity distribution [3]. Characterizing droplet deformation during the breakup is critical for understanding the physics and ultimate atomized distribution for these engineering applications. However, deformation is usually a dynamic three-dimensional (3D) process with complex geometries [4] that are challenging to capture with prevalent planar techniques [5]. Recently tomographic (3D) spray reconstructions have been demonstrated with various techniques: X-rays [6], back-illumination [7], and fluorescence [8]. These methods use multiple camera perspectives to algorithmically reconstruct the target spray based on the captured intensity information from each technique. Digital inline holography (DIH) is another three-dimensional measurement technique commonly used to determine the shape, size, and location of small objects with high-resolution [9–13]. With adequate time-resolution, holographic measurements may be combined with advanced processing methods [14] to extract additional 3D velocities [15,16]. Hence, DIH is potentially a viable alternative to resolve the complex 3D droplet deformation process in engineering applications when high resolution.

When a collimated coherent light passes an object field, the light that is disturbed by the liquid or solid objects will superimpose with the undisturbed light at the imaging plane of the camera, forming an interference pattern (hologram) due to their phase variation. Thus, unlike traditional imaging techniques, DIH records interference patterns of the targets instead of a focused image. The phase information encoded in the interference patterns is used to retrieve the target's location in the light propagation direction. That is, with just one hologram, DIH can record the projected cross section of the target and the relative distance between the camera and the target. Adequate time-resolution may also be used for velocity measurements [3,17]. However, the DIH reconstruction produces lower and higher levels of uncertainty between the in-plane (parallel to the hologram/camera plane) and out-of-plane (normal to the hologram/camera plane), respectively. Complexities encountered in traditional holographic techniques, such as "twin imaging," is overcome with the "inline" arrangement, significantly simplifying the experimental setup. When measuring complex structures, DIH omits the overlapping features since the interference patterns are merged; hence, standard DIH is typically limited to optically thin sprays. To resolve these issues, algorithmic improvements are able to separate the overlapped edges (e.g., the "hybrid method") [18]. Still, if portions of the target are blocked completely, there is no means of reconstructing them because of the lack of captured information. To collect the blocked information, an additional perspective is needed, much like tomographic techniques. Previous works have demonstrated particle size and velocity measurement by applying up to three DIH reconstruction directions [17,19]. However, previous applications of multiple DIH directions have focused primarily on overcoming the out-of-plane uncertainty limitations for simple spherical geometries [10,17,19].

In this work, the multiview (≥ 3) DIH is applied to a target model whose shape simulates a complex structure formed in a typical breakup process of a liquid drop. Unlike the prior work by

[1]Corresponding author.

Contributed by the Fluids Engineering Division of ASME for publication in the Journal of Fluids Engineering. Manuscript received October 31, 2021; final manuscript received January 12, 2022; published online February 28, 2022. Editor: Francine Battaglia.

Soria and Atkinson [17], the target model used for this experiment possesses a larger dimension liquid surface and a nonspherical multiple ligaments and droplets geometry. Critically, the reconstruction based on the intensity volume, proposed by Soria and Atkinson, is invalid for this case because of the size of the test model (the result does not represent the true geometry), and an alternative approach is proposed. First, the outlines and the cross section of the target are determined via DIH from the holograms recorded in each view. Then two reconstruction methods, the outline-based and cross section-based methods, are applied to reconstruct the geometry of the target model individually. The outline-based method combines all the outlines of the target measured from different views to estimate the shape of the target. The cross section-based method follows the same approach as tomography and reconstructs the target using the projection of the target cross section from different views. The results demonstrate how multiview DIH can be used to reconstruct a complex droplet breakup model about 2 mm × 2 mm × 4 mm in size.

2 Measurement Principle

The multiview DIH reconstruction is comprised of two parts: first, extract the useful information from the holograms recorded at each view, and second, combine the information gathered from each view to estimate the geometry of the target. The first part is already a well-developed technique for DIH; thus, this paper will focus on the second part: how to combine the information from each view to estimate the geometry of the test target. A brief review of the DIH reconstruction principle is first discussed below, followed by two proposed target reconstruction methods demonstrated initially on a simple triangular prism-like geometry.

2.1 Digital Inline Holography Recording and Reconstruction. A typical DIH setup contains a laser source, a spatial filter, collimating lenses, a magnifying lens, and a digital camera. The laser beam first passes the spatial filter and the collimating lenses to form a diffraction-free collimated beam. When the beam passes through the test model, a hologram is generated and recorded by a digital camera aligned with the laser beam. It may be resized before the camera by a magnifying lens. For this experiment, the static test model is mounted on a rotation stage enabling different perspectives of the model, as shown in Fig. 1. In future applications for dynamic measurements, the multiview DIH recording can be performed by using multiple cameras to record holograms from different viewing angles. Once the beam passes the collimating lenses, it can be treated as a plane wave whose electric field amplitude, a_R, is uniform perpendicular to the propagation direction. When the beam reaches the model, the light is partially blocked and diffracted by the edges of the model. Among the planes normal to the light propagation direction, the object (ξ, η) and hologram planes (x, y) are defined where diffraction occurs and where the hologram is recorded, respectively, as shown in Fig. 2. Based on the Fresnel-Kirchhoff integration, which quantitatively describes the electric field in the space caused after diffraction [20], the electric field at the object plane $\Gamma(\xi, \eta)$ can be reconstructed by the recorded hologram $h(x, y)$

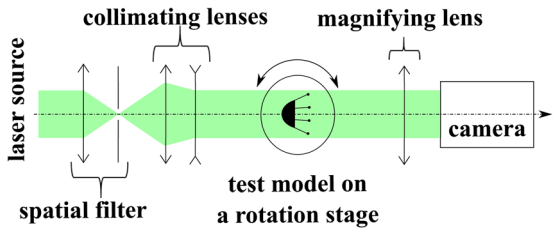

Fig. 1 Schematic of multiview DIH recording

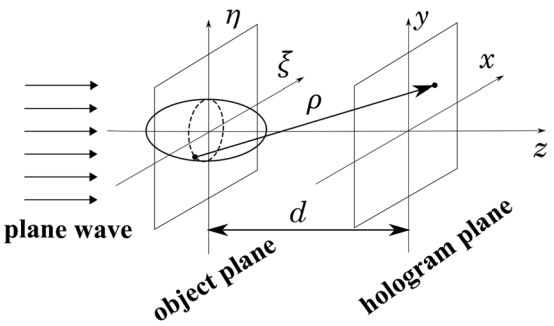

Fig. 2 Illustration of the coordinates for hologram reconstruction

$$\Gamma(\xi,\eta) = \frac{i}{\lambda}\int_{-\infty}^{+\infty}\int_{-\infty}^{+\infty} h(x,y)a_R \frac{\exp(-i\cdot 2\pi\cdot\rho/\lambda)}{\rho}dxdy \tag{1}$$

with

$$\rho = \sqrt{(x-\xi)^2 + (y-\eta)^2 + d^2} \tag{2}$$

where λ is the wavelength of the beam and d is the distance between the two planes. As shown in Eq. (2), ρ represents the distance between two arbitrary points on the hologram plane and the object plane. However, Eq. (1) is computationally expensive, and the Fresnel approximation is typically used [20]. Accordingly, when the $x - y$ or $\xi - \eta$ ranges are small compared to the reconstruction distance d, then ρ can be approximated with the first few terms of its Taylor series

$$\rho = d + \frac{(\xi - x)^2}{2d} + \frac{(\eta - y)^2}{2d} \tag{3}$$

Therefore, Eq. (1) can be rewritten in the Fresnel approximation form as

$$\begin{aligned}\Gamma(\xi,\eta) = {} & \frac{i}{\lambda d}\exp\left(-i\frac{2\pi d}{\lambda}\right)\exp\left[-i\frac{\pi(\xi^2+\eta^2)}{\lambda d}\right] \\ & \times \int_{-\infty}^{+\infty}\int_{-\infty}^{+\infty} h(x,y)a_R \exp\left[\frac{-i\pi(x^2+y^2)}{\lambda d}\right] \\ & \exp\left[\frac{i2\pi(x\xi+y\eta)}{\lambda d}\right]dxdy\end{aligned} \tag{4}$$

Equation (4) is similar in form to the Fourier transform and thereby can be calculated in the frequency domain. This boosts the computational speed when reconstructing the discretized field at the object plane from the recorded hologram. With reconstructions at various distances from the hologram plane, the intensity field at each d is acquired by

$$I(\xi,\eta) = |\Gamma(\xi,\eta)|^2 \tag{5}$$

The edge of the test model can then be determined by identifying a reconstruction distance (d) that results in the sharpest edge. In other words, when a model edge (x, y) is in focus by the reconstructed image location (d), DIH locates the target edge in 3D space (x, y, d). In principle, when the light propagates away from the object plane, the diffraction patterns grow proportional to the propagation distance. The focused image location is found when there are no diffraction patterns at the edge and is defined as the focal plane. Notably, the edge of the target may not be in focus at the single focal plane but rather at multiple focal planes. In other words, different target edges may be in focus at different reconstruction distances. By pairing each edge point with different d,

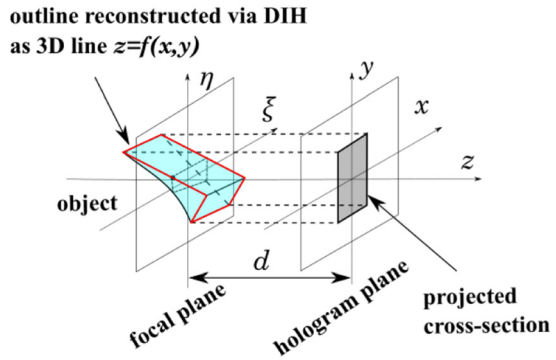

Fig. 3 Outline and cross section reconstructed via DIH at a selected view

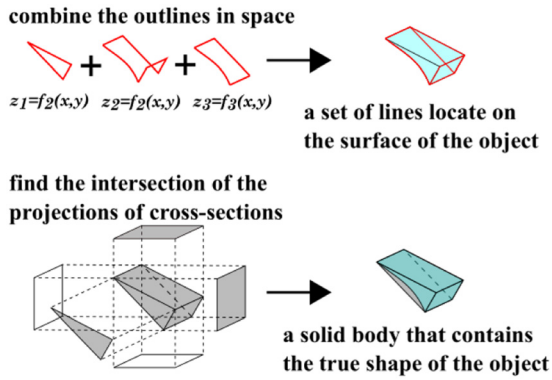

Fig. 5 Two methods to estimate the geometry of the test object

the 3D outline of the target model is determined. In this work, Yao's method [11] is used to generate the 3D outlines of nonspherical structures, in which a wavelet transform is used to identify the focal plane from the DIH reconstructions.

2.2 Geometric Reconstruction. In addition to the DIH outline, shadowgraphs can be built by combining all the focused parts of the reconstructions at different distances. With the shadowgraph, the projected cross section of the test model is thereby determined. An illustration of the relationship between the outline (marked as red line) and the projected cross section (marked as gray shadow) of a triangular prism model is shown in Fig. 3 from a selected view. The outline function can be expressed as $z = f(x, y)$ for each point (x, y) along the outline. Here, z is determined from the reconstruction distance, d, with the highest sharpness for the corresponding edge. Extending this procedure to multiple views from different orientations, each perspective contains unique information about the test target. This is demonstrated in Fig. 4 for a triangular prism with a modified complex edge. Each perpendicular perspective contains unique information about the model in either the outlines, cross section, or both.

Both cross section and outlines can be used to estimate the model shape individually, as demonstrated in Fig. 5. Before the geometric reconstruction, all the cross section and outlines must be transformed from individual camera/hologram coordinates into model space. In practice, a calibration plate of known dimensions is used as a reference in the test section and is typical of multicamera arrangements [6–8,21,22]. Therefore, the calibration plate location defines the coordinates in model space.

The cross section-based reconstructions estimate the model geometry by intersecting the projections from the multiple views. The result is a solid body that encloses the true geometry of the target analogous to a convex hull. Depending on the model and view directions, portions of the target may be blocked in certain views, and the blocked information would be omitted in the reconstructions. For example, in Fig. 4, the view 2 cross section is triangular even though the two parallel sides of the prism are not identical. As a result, the extracted cross section only represents the shape of one side, but the reconstruction geometry estimates both sides as triangular.

On the other hand, the outline-based method does not necessarily generate an enclosed volume. The shape of the test model is estimated when combining the outlines in space, but key enclosing lines may be omitted depending on the number of views and orientations. In Fig. 4, the known outlines are in red and the blocked edge, not found from the DIH process, is marked in blue. However, estimating a solid body from a set of 3D outlines is quite challenging since the possible solution is not unique (it is an ill-posed problem).

In this work, a method that utilizes the extracted outlines (or points, if discretized) is proposed to estimate the model geometry. The proposed method is implemented with the following steps: (1) choose a slicing direction in the model coordinate system, the y-axis highlighted in Fig. 6 is used here; (2) create a plane normal

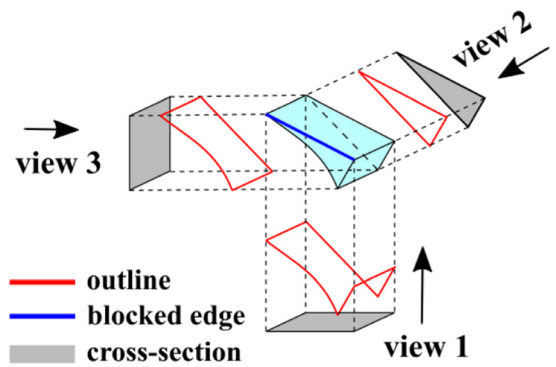

Fig. 4 Outline and cross section reconstructed from multiple views

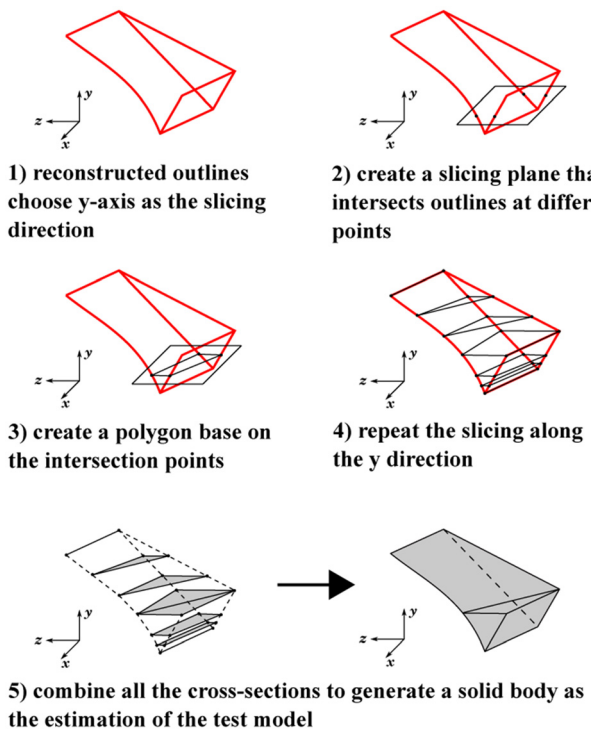

Fig. 6 Estimation of the test model geometry with the outlines reconstructed by DIH

to the slicing direction at an arbitrary height y and find the intersection between the slicing plane and the outlines (i.e., find the points on the slicing plane where the outlines intersect it); (3) determine a polygon whose vertices are made of the intersection points, assuming the polygon estimates the cross section of the model in the slicing plane; (4) repeat steps 1–3 to find the estimated cross section at each y; and (5) combine all the cross section to build an estimation of the test model. The reconstruction process listed above is depicted in Fig. 6. Mathematically, each estimated cross section has no thickness, and the slicing interval should be infinitely small. However, a discretization of the slicing process is applied by assigning each slicing plane a thickness. Thus, at each plane, a solid body is generated by extruding the specified polygon, and the combination of extrusions reconstructs the final estimation of the model.

Some details need to be stressed for the proposed method. First, there are multiple choices of the slicing direction. The optimal direction should be perpendicular to the direction of the majority recording views. For example, in Sec. 4, all the view directions are perpendicular to the rotation axis of the test model, thus, the slicing direction is chosen to be parallel to the rotation axis. This direction maximizes the contiguity of the estimating polygons in the slicing direction. Therefore, the chance to estimate a smooth profile is maximized by avoiding a slicing plane parallel to an outline and consequently distributing intersection points across the multiple slicing planes. Second, since those intersection points are from the outlines, which means they are on the surface of the model, the polygons estimated by those points are the ones whose vertices are made by them. Therefore, different connection orders of those points determine different polygons and those polygons may not necessarily be convex polygons. In this work, the polygon used to estimate the test model is chosen to have the maximum area among all possible polygons. Third, when selecting the maximum-area polygon with a set of intersection points in a certain slicing plane, the number of polygons is the permutation of the points regardless of the starting point and the starting direction of the connection, e.g., for n points there are $(n-1)!/2$ possible polygons. Comparing the areas of $(n-1)!/2$ polygons may easily fill the memory of a standard laptop. For this reason, the slicing direction must be chosen carefully to avoid too many points shown in one slicing plane. However, the polygon with the maximum area usually has the minimum perimeter. Since the computational cost for the perimeter is much cheaper than the area, perimeters are used in the topological polygon optimization. Finally, unlike the cross section-based method whose estimation always encloses the true geometry of the model, the outline-based method may underestimate or overestimate the true geometry volume. The example shown in Fig. 6 is a case that the reconstruction is enclosed (underestimated) by the true geometry. However, for the same outlines, if the slicing direction along with the x-axis is used, the reconstruction would then enclose (overestimate) the true geometry.

3 Experimental Setup

The multiview DIH setup is shown in Fig. 7, including the calibration target and test model. The coherent light is generated from the laser source (CiviLaser—LSR532NL—600, $\lambda = 532$ nm, 0.3 W) then passes the spatial filter and collimating lenses to form the diffraction-free beam. When the beam passes the test section, the hologram is generated and projected to the camera (FLIR, Wilsonville, OR, Grasshopper3 GS3-U3-32S4M, resolution: 2048×1536) via a magnifying lens. The test section is located on a rotation stage to enable the recording of different views of the test model and calibration target for reference. The calibration target (Grid Distortion Target, Thorlabs R2L2S3P1, pattern size 25 mm × 25 mm, 125 μm spacing) mounted on a 3-axis translation stage is used for calibrating the coordinates between different views and the DIH reconstruction distance. A 3D printed test model is used to simulate the structure of a droplet breakup and

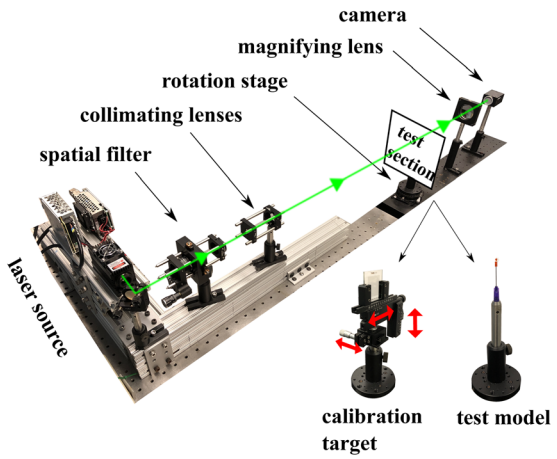

Fig. 7 Setup for multiview DIH

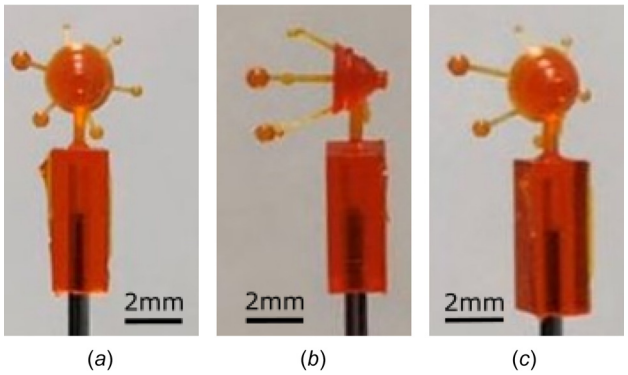

Fig. 8 3D printed test model simulating a droplet breakup event: (*a*) front view, (*b*) side view, and (*c*) isometric view

evaluate the measurement capability of the proposed method. The printed model is shown in Fig. 8 and a sketch with dimension is shown in Fig. 9. The diameter of the cone structure at the front is around 2 mm and the diameters of droplets on the rear of the branches range from 0.2 to 0.6 mm. Notably, the printed model is slightly different from the specified dimensions due to manufacturing defects. The front view is defined as the 0 deg angle, shown in Fig. 8(*a*). Using the rotation stage, the holograms of the test model are recorded from multiple viewing angles ranging from 0 deg to 360 deg with 5 deg intervals.

4 Results and Discussion

Figures 10(*a*) and 10(*b*) show an example hologram recorded by the DIH system at a viewing angle at 120 deg and its DIH reconstructed image, respectively. The zoomed portion in Fig. 10 demonstrates the reconstructed image has a sharp edge in

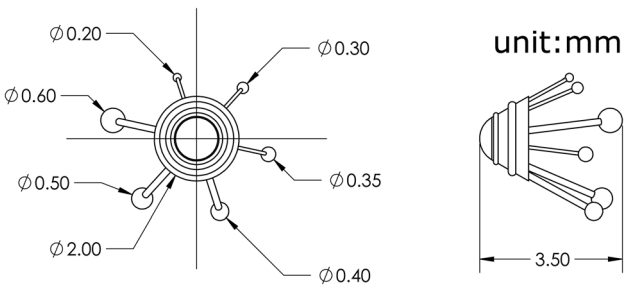

Fig. 9 Test model drawing with key dimensions labeled

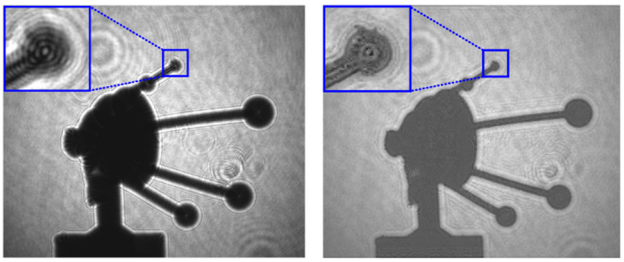

Fig. 10 A representative hologram and corresponding reconstruction of the test model at 120 deg. The 0.2 mm sphere is highlighted: (*a*) hologram and (*b*) reconstruction.

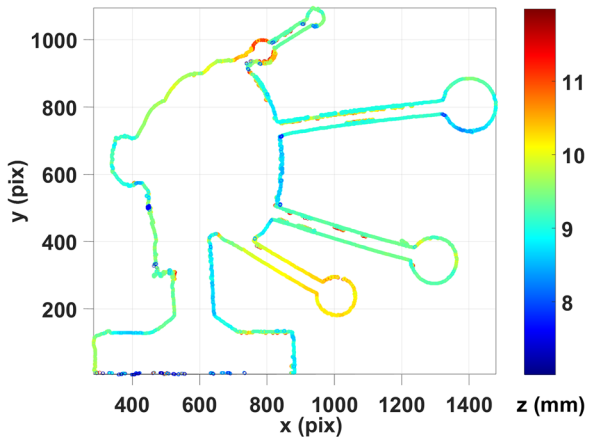

Fig. 11 The resulting outline at 120 deg. The color bar indicates the outline's location, *z*, relative to the hologram plane.

comparison to the hologram. Additionally, some printer defects are visible which act as a source of noise for the boundary estimation. The corresponding outline for the 120 deg hologram is shown in Fig. 11. The outlines of the spheres at each branch and their supporting structures are obtained in z as the distance to the hologram plane. The top two branches, in particular, are separated by the DIH reconstruction in the out-of-plane direction even though one sphere is overlapped with another branch. Once the outline is identified, the cross section is then determined via postprocessing as discussed in Sec. 2.2 (Fig. 12).

Here, the 25 deg, 120 deg, and 210 deg angles are used to estimate the model geometry. The extracted 3D outlines are demonstrated as the discretized points in Figs. 13(*a*) and 13(*b*), profile

Fig. 12 The resulting projected cross section at 120 deg

the true model shape. However, some smearing of the outline is visible in the orange profile (Fig. 13(*a*); 120 deg). DIH has larger uncertainties in the z-direction, and hence some distribution/smearing of the estimated outline is expected. The resulting reconstruction results of the outline-based method are depicted in Figs. 13(*c*) and 13(*d*). Notably, along the height direction, the estimated polygon of each slice is not smooth. This is due to the model and camera orientations resulting in a different number of points at each slicing plane. In other words, at one height, there might be enough points to give a precise estimation, and the next slice yields a poor estimation because of a lack of points. The result is a sudden change of the polygon shapes between the adjacent slices. This is primarily an artifact of the discretized reconstruction method: a continuous border function, in contrast, has defined intersections at all slice planes. Additionally, the branches are merged and reconstructed as one piece. In the cross section-based method, shown in Figs. 13(*e*) and 13(*f*), the reconstructed geometry is a contiguous solid body with additional extrusions in comparison to the real geometry of the model. The spheres on the top are reconstructed as cylinders, and the branches, especially the ones in the middle, are reconstructed as plates instead of rods. In general, using only three views, the outline-based and cross section-based test model reconstructions lack accuracy, with the former more severe than the latter. However, the cross section-based method guarantees a continuous geometry. Therefore, a larger number of views is necessary to faithfully reconstruct complex droplet deformation-like geometries.

Increasing the number of views should asymptotically improve the reconstructed estimate accuracy toward the true solution [6,23]. Figure 14 demonstrates the reconstruction results of the cross section-based method with a different number of views that evenly distributed between 0 deg to 180 deg. As the used views increase, the reconstructed results gradually approach the true geometry of the droplet model with diminishing returns for higher view counts. Most of the improvement on the reconstruction accuracy is achieved from the first six views: Fig. 15 demonstrates more details of a six-view reconstruction (from 0 deg to 150 deg with an interval of 30 deg) where the spheres are no longer elongated to cylinders and the top/bottom branches are no longer reconstructed as plates. However, when looking from the top view (Fig. 15(*d*)), the branches in the middle of the model are still reconstructed as plates since that region remained blocked by the cone of the test model. Consequently, continuing to add views does not significantly improve the reconstruction (Fig. 14). The same asymptotic trend is observed from the outline-based-reconstructions depicted in Fig. 16. Even with a different reconstruction methodology, the merging issue of the branches is not resolved. This limitation implies that multiview DIH reconstructions may not resolve concave or hollow structures due to information lost via blocking.

The relative volume and accuracy are used to quantify the effect of the number of views used in the two reconstruction methods. Since the droplet model is 3D printed with errors, the true geometry of the model is unknown. Thus, the reconstructed result of thirty-six views via the cross section-based method is used as a datum for comparison representing the true solution (e.g., the relative volume is the volume of the reconstructed model normalized by the datum volume). Figure 17(*a*) depicts the normalized reconstructed volume for a different number of input views. The cross section-based method volume decreases with more views as expected since the "convex-hull" is minimized toward the true solution with additional constraints. The opposite trend is apparent in the outline-based reconstructions; more views result in more outlines, and thus, the larger model is reconstructed in general. However, recalling step 3 of the outline-based reconstruction process, finding more points will not necessarily extend the size of the polygon (e.g., quadrilaterals generated by adding a point inside and outside of the same triangle). Thus, there are exceptions where more views decrease the reconstructed volume: this is demonstrated by the nine-view case of the outline-based method

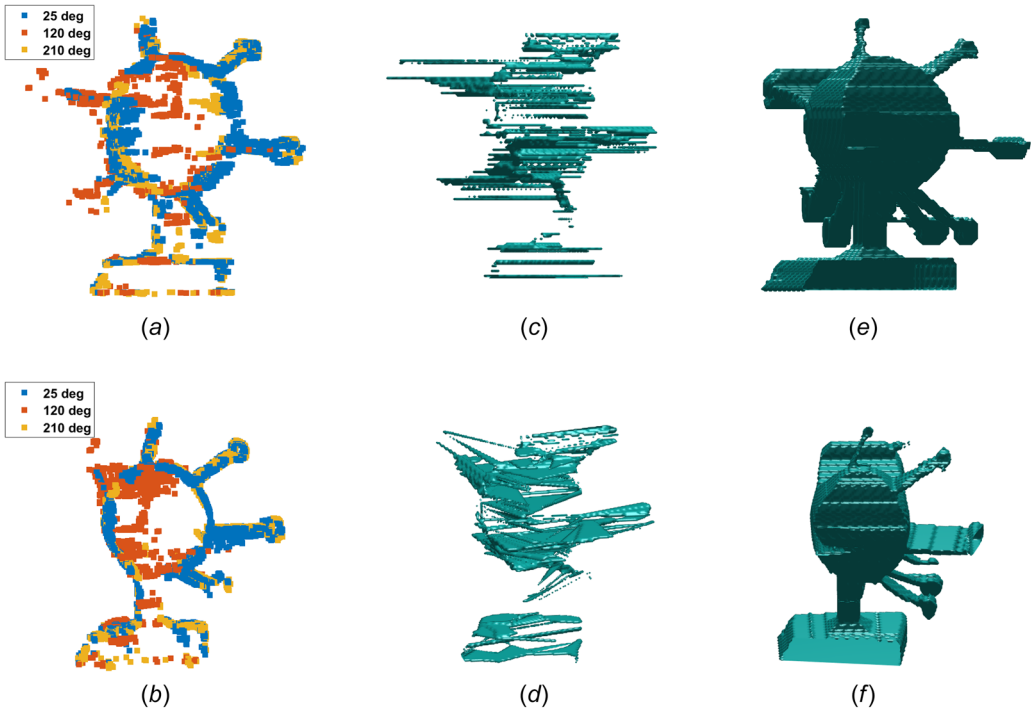

Fig. 13 Object geometry reconstructions based on the recording angles at 25 deg, 120 deg, and 210 deg: (*a*) discretized outlines at the front view; (*b*) discretized outlines at the isometric view; (*c*) outline-based method result at the front view; (*d*) outline-based method result at the isometric view; (*e*) cross section-based method result at the front view; and (*f*) cross section-based method result at isometric view

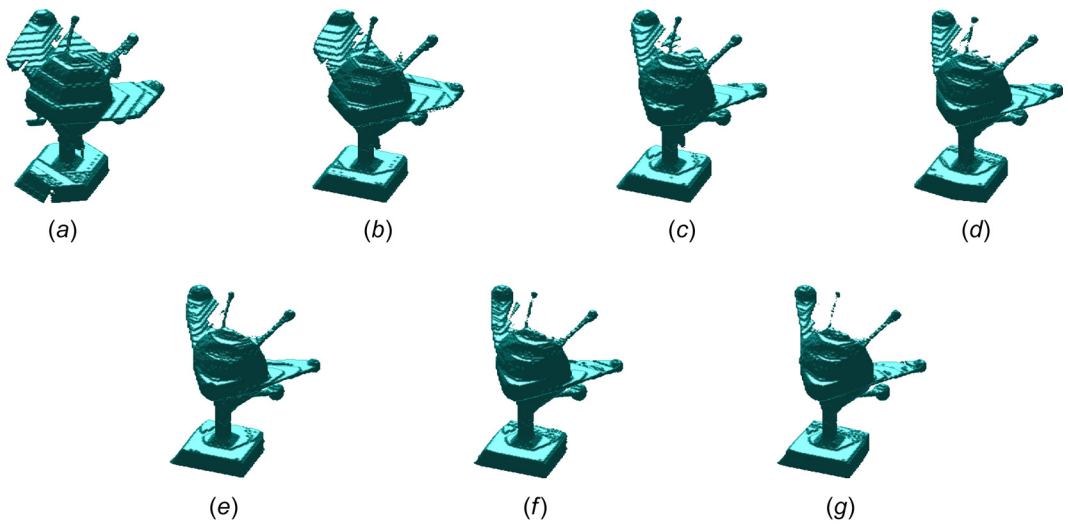

Fig. 14 Reconstruction via cross section-based method under different numbers of viewing direction: (*a*) 3 views with the interval of 60 deg, (*b*) 4 views with the interval of 45 deg, (*c*) 6 views with the interval of 30 deg, (*d*) 9 views with the interval of 20 deg, (*e*) 12 views with the interval of 15 deg, (*f*) 18 views with the interval of 10 deg, and (*g*) 36 views with the interval of 5 deg

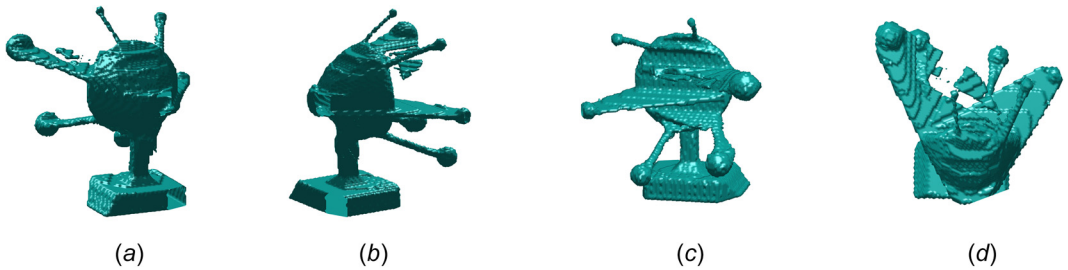

Fig. 15 Cross section reconstruction based on the recording angle at 0 deg, 30 deg, 60 deg, 90 deg, 120 deg, and 150 deg, respectively: (*a*) front view 1, (*b*) front view 2, (*c*) back view, and (*d*) top view

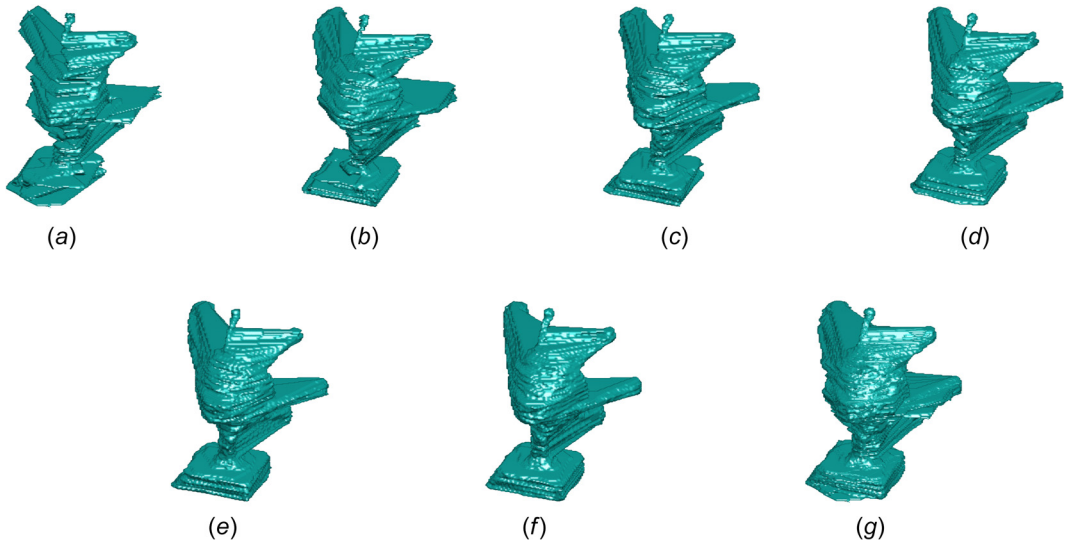

Fig. 16 Reconstruction via outline-based method under different numbers of viewing direction: (*a*) 3 views with the interval of 60 deg, (*b*) 4 views with the interval of 45 deg, (*c*) 6 views with the interval of 30 deg, (*d*) 9 views with the interval of 20 deg, (*e*) 12 views with the interval of 15 deg, (*f*) 18 views with the interval of 10 deg, and (*g*) 36 views with the interval of 5 deg

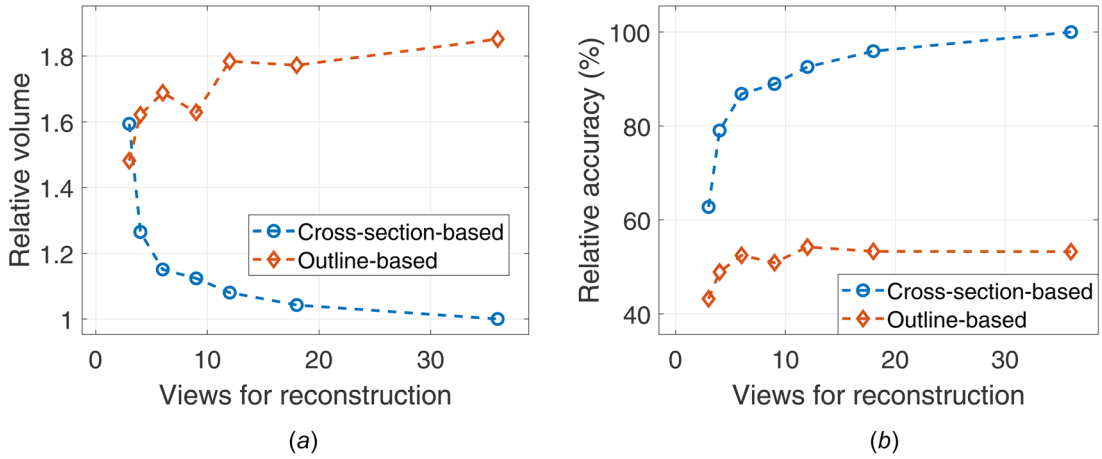

Fig. 17 Relative (*a*) volume and (*b*) accuracy of resultant reconstructions using different numbers of viewing directions. The cross-section-based reconstruction with 36 views is used as the datum.

in Fig. 17(*a*). Overall, the outline-based reconstructions are inherently limited and the accuracy asymptotes in the order of 50% (Fig. 17(*b*)). The cross section-based method is significantly more capable and a ≈90% accuracy is expected with at least nine views. Although the datum still has a larger volume than the true solution because of the branches in the middle of the model, they are a small fraction of the total volume and may be neglected. Therefore, Fig. 17(*b*) serves as a reference of the reconstruction accuracies possible with view totals. Ultimately, the reconstruction accuracy is dependent on the number of viewing directions, viewing angles, and camera calibration accuracy akin to the analysis of Elsinga et al. for solid particle fields [23]. For multiview digital inline holography, however, the accuracy also depends on the concavity and resulting blocked/shadowed regions of the structure.

5 Conclusions

This research demonstrates the capability of using the multiview DIH technique to measure a test model with a complex shape. The 3D outlines and the cross section are first determined via DIH reconstructions from each view, then the geometric reconstructions of the test model obtained via two methodologies are evaluated. The outline-based method estimates the model geometry by generating a polygon cross section from the 3D outlines; the cross section-based method generates an envelope of the geometry from the various projections.

The outline-based reconstructions are limited in practice–because of the out-of-plane DIH uncertainty in the discretized outlines, it does not guarantee a solid volume, and it cannot separate concave structures (e.g., nonconnected branches in the test model). The cross section-based reconstruction can estimate the test model envelope (convex hull) with a solid body, but concave structures are still limited. Overall, the more views are used with unique information about the model, the more accurate the reconstructions become. However, a cross section reconstruction doesn't require the DIH setup; It also can be achieved via a traditional tomographic setup such as the shadowgraph technique [7]. Notably, DIH may provide advantages especially when high spatiotemporal resolution is desired. Compared to the cross section-based method, the outline-based method acquires

additional information and results in less accurate reconstructions due to practical limitations. However, a single outline contains more information about the target than a cross section, and hence combing the two methods may yield better reconstructions with a fractional number of views: developing a hybrid method is a topic for future work. However, improved reconstruction algorithms are still limited by the lack of information from blocked structures, thus multiview DIH may not be appropriate where concave or hollow structures are expected.

Funding Data

- Office of Naval Research Grant No. N68335-20-C-0432ONR (Funder ID: 10.13039/100000006) (Eric Marineau, Program Manager).

Nomenclature

a_R = amplitude of the plane wave
d = reconstruction distance
h = hologram
I = intensity of the reconstructed image
n = number of points in a slicing plane
x, y, z = coordinates on hologram plane
Γ = reconstructed intensity field
λ = wavelength of light source
ξ, η = coordinates on object plane
ρ = distance between points on object and hologram planes

References

[1] Lefebvre, A. H., and Mcdonell, V. G., 2017, *Atomization and Sprays*, 2nd ed., CRC Press, Portland, OR.
[2] Gad-El-Hak, M., 2016, "Nine Decades of Fluid Mechanics," ASME J. Fluids Eng., **138**(10), p. 100802.
[3] Obenauf, D., Yao, L., Shang, W., Sojka, P. E., and Chen, J., 2019, "Effect of Reduced Surface Tension on Size and Velocity Distributions of Ethanol-Water Drop Fragments Formed Via Multi-Mode and Sheet-Thinning Breakup," AIAA Paper No.2019-4333.
[4] Guildenbecher, D. R., López-Rivera, C., and Sojka, P. E., 2009, "Secondary Atomization," Exp. Fluids, **46**(3), pp. 371–402.
[5] Fansler, T. D., and Parrish, S. E., 2015, "Spray Measurement Technology: A Review," Meas. Sci. Technol., **26**(1), p. 012002.
[6] Halls, B. R., Rahman, N., Slipchenko, M. N., James, J. W., McMaster, A., Ligthfoot, M. D. A., Gord, J. R., and Meyer, T. R., 2019, "4D Spatiotemporal Evolution of Liquid Spray Using Kilohertz-Rate x-Ray Computed Tomography," Opt. Lett., **44**(20), pp. 5013–5016.
[7] Du, J., Zang, G., Mohan, B., Idoughi, R., Sim, J., Fang, T., Wonka, P., Heidrich, W., and Roberts, W. L., 2020, "Study of Spray Structure From Non-Flash to Flash Boiling Conditions With Space-Time Tomography," Proc. Combust. Inst., **06**(17), pp. 1–9.
[8] Gomez, M., Braun, A. M., Slipchenko, M. N., Roy, S., and Meyer, T. R., 2022, "Time-Resolved Volumetric (4D) Laser-Induced Fluorescence Imaging of Primary Spray Breakup," AIAA SciTech 2022 Forum, San Diego, CA, pp. 1–10.
[9] Gao, J., Guildenbecher, D. R., Reu, P. L., Kulkarni, V., Sojka, P. E., and Chen, J., 2013, "Quantitative, Three-Dimensional Diagnostics of Multiphase Drop Fragmentation Via Digital in-Line Holography," Opt. Lett., **38**(11), pp. 1893–1895.
[10] Guildenbecher, D. R., Gao, J., Chen, J., and Sojka, P. E., 2017, "Characterization of Drop Aerodynamic Fragmentation in the Bag and Sheet-Thinning Regimes by Crossed-Beam, Two-View, Digital in-Line Holography," Int. J. Multiphase Flow, **94**(C), pp. 107–122.
[11] Yao, L., Chen, J., Sojka, P. E., Wu, X., and Cen, K., 2018, "Three-Dimensional Dynamic Measurement of Irregular Stringy Objects Via Digital Holography," Opt. Letters, **43**(6), pp. 1283–1286.
[12] Kumar, S. S., Li, C., Christen, C. E., Hogan, C. J., Fredericks, S. A., and Hong, J., 2019, "Automated Droplet Size Distribution Measurements Using Digital Inline Holography," J. Aerosol Sci., **137**, p. 105442.
[13] Yu, P.-W., and Ceccio, S. L., 1997, "Diffusion Induced Bubble Populations Downstream of a Partial Cavity," ASME J. Fluids Eng., **119**(4), pp. 782–787.
[14] Ezra, E., Keinan, E., Liberzon, A., and Nahmias, Y., 2016, "Development of Three-Dimensional Streamline Image Velocimetry Using Superimposed Delaunay Triangulation and Geometrical Fitting," ASME J. Fluids Eng., **138**(1), p. 011205.
[15] Li, X. B., Oishi, M., Matsuo, T., Oshima, M., and Li, F. C., 2016, "Measurement of Viscoelastic Fluid Flow in the Curved Microchannel Using Digital Holographic Microscope and Polarized Camera," ASME J. Fluids Eng., **138**(9), p. 091401.
[16] Guildenbecher, D. R., Cooper, M. A., and Sojka, P. E., 2016, "High-Speed (20 kHz) Digital in-Line Holography for Transient Particle Tracking and Sizing in Multiphase Flows," Appl. Opt., **55**(11), p. 2892.
[17] Soria, J., and Atkinson, C., 2008, "Towards 3C-3D Digital Holographic Fluid Velocity Vector Field Measurement–Tomographic Digital Holographic PIV (TOMO-HPIV)," Meas. Sci. Technol., **19**(7), p. 074002.
[18] Gao, J., Guildenbecher, D. R., Reu, P. L., and Chen, J., 2013, "Uncertainty Characterization of Particle Depth Measurement Using Digital In-Line Holography and the Hybrid Method," Opt. Exp., **21**(22), pp. 26432–26449.
[19] Buchmann, N. A., Atkinson, C., and Soria, J., 2012, "Ultra-High-Speed Tomographic Digital Holographic Velocimetry in Supersonic Particle-Laden Jet Flows," Meas. Sci. Technol., **24**(2), p. 24005.
[20] Schnars, U., 2005, *Digital Holography Digital Hologram Recording, Numerical Reconstruction, and Related Techniques*, 1st ed., Springer, Berlin, Germany.
[21] Lauriola, D., Meyer, T. R., Gomez, M., Roy, S., Slipchenko, M. N., Gord, J. R., and Son, S. F., 2018, "KHz–MHz Rate Laser-Based Tracking of Particles and Product Gases for Multiphase Blast Fields," 2018 IEEE Research and Applications of Photonics in Defense Conference (RAPID), IEEE, Miramar Beach, FL, Aug. 22–24, pp. 1–4.
[22] Lauriola, D. K., Gomez, M., Meyer, T. R., Son, S. F., Slipchenko, M., and Roy, S., 2019, "High Speed Particle Image Velocimetry and Particle Tracking Methods in Reactive and Non-Reactive Flows," AIAA Paper No. 2019-1605.
[23] Elsinga, G. E., Scarano, F., Wieneke, B., and Van Oudheusden, B. W., 2006, "Tomographic Particle Image Velocimetry," Exp. Fluids, **41**(6), pp. 933–947.